Enhancing hydrogen peroxide activation of Cu-Co layered double hydroxide by compositing with biochar: Performance and mechanism

Ling Li [a], Min Cheng [a], Lei Qin [a], Eydhah Almatrafi [b], Xiaofeng Yang [a], Lu Yang [a], Chensi Tang [a], Shiyu Liu [a], Huan Yi [a], Mingming Zhang [a], Yukui Fu [a], Xuerong Zhou [a], Fuhang Xu [a], Guangming Zeng [a,b,*], Cui Lai [a,*]

[a] College of Environmental Science and Engineering and Key Laboratory of Environmental Biology and Pollution Control (Ministry of Education), Hunan University, Changsha, 410082, PR China

[b] Center of Research Excellence in Renewable Energy and Power Systems, Center of Excellence in Desalination Technology, Department of Mechanical Engineering, Faculty of Engineering-Rabigh, King Abdulaziz University, Jeddah 21589, Saudi Arabia

* Corresponding author.
E-mail address: zgming@hnu.edu.cn (G.M. Zeng) and laicui@hnu.edu.cn (C.Lai).

Abstract

In this study, Cu-Co layered double hydroxide/biochar composite (Cu-Co LDH/BC) was prepared and employed for activating H_2O_2 to degrade ciprofloxacin (CIP), a common fluroquinolone antibiotic detected in water environment. The as-synthesized catalysts were also comprehensively characterized to study the physiochemical properties. For the catalytic activity, the degradation rate of Cu-Co LDH/BC to CIP was approximately 1.5 times higher than that of Cu-Co LDH. The improved catalytic activity can be ascribed to the synergistic effect between Cu-Co LDH and BC, such as more functional groups, accelerated electron transfer, and varied charge distribution. Meanwhile, Cu-Co LDH/BC/H_2O_2 could degrade CIP efficiently in a wider pH range comparing with Cu-Co LDH/H_2O_2, and the efficiency was approximately 84.7% at neutral pH within 90 min. The generation of $^{\bullet}OH$, $O_2^{\bullet-}$ and $^1O_2$ in Cu-Co LDH/BC/H_2O_2 system were then verified by electron spin resonance (ESR) technology. The quenching experiments indicated that both non-radical pathway ($^1O_2$) and radical pathway ($^{\bullet}OH$, $O_2^{\bullet-}$) led to CIP degradation, in which $O_2^{\bullet-}$ and $^1O_2$ made major contribution. Then, the intermediate products of CIP during catalytic reaction were monitored by high-performance liquid chromatography-mass spectrometry (HPLC-MS), and the environmental risk of these degradation intermediates was tested through seed germination experiments. This study tends to provide valuable information for LDH/BC application in heterogeneous Fenton-like reaction.

Keywords: Layered double hydroxide, biochar, H_2O_2 activation, antibiotic, water treatment

1. Introduction

Ciprofloxacin (CIP) is a kind of fluoroquinolone antibiotics used worldwide for treating human and livestock diseases via inhibiting enzyme activity. Nevertheless, CIP cannot be metabolically decomposed entirely, resulting in most of them discharging into environment through urine and feces, then flowing into water environment (Lu et al. 2020). For this reason, CIP can be usually detected in municipal wastewater and pharmaceutical wastewater with concentration around 14 mg/L and 31 mg/L, respectively (Table S1). The presence of CIP in water sources is susceptible to induce the appearance of resistant bacteria even at extremely low concentrations. Therefore, developing efficient strategies to eliminate CIP from water environment is necessary.

Advanced oxidation technologies (AOPs) are recognized as promising techniques for treating various recalcitrant organic pollutants (Li et al. 2022a, Zhang et al. 2020). Among various AOPs (i.e., photocatalysis, thermal treatment, Fenton process, and persulfate-based oxidation) (Li et al. 2022b, Sun et al. 2019, Sun et al. 2020, Wang et al. 2020a), Fenton process consisting of H_2O_2 activation has been considered as an attractive technology in wastewater treatment owing to its strong oxidation ability, simple device requirements, and environment-friendly products of H_2O_2 decomposition (H_2O and O_2) (Liu et al. 2021, Yan et al. 2021). Regrettably, although homogeneous Fenton process with soluble Fe^{2+} as catalyst possesses powerful oxidation capacity, it still faces several limitations, including accumulation of Fe-containing sludge, narrow working pH (pH 2.8-3.5), and difficulty in catalyst recycling (Lai et al. 2019, Li et al. 2019). To this end, many researches are attempting to develop heterogeneous Fenton-

like catalysts to activate H_2O_2 for overcoming the above drawbacks.

Lately, layered double hydroxide (LDH), a typical metal-based material consisting of positively charged metal hydroxide layers with water molecules and anions intercalated between the layers, has attracted extensive attention as Fenton-like catalyst because of its unique layered structure, composition as well as relatively simple fabrication process (Guo et al. 2020, Ye et al. 2020, Yi et al. 2021). To be specific, various bivalent and trivalent transition metal ions can be evenly and orderly dispersed into the LDH layers, which endow LDH the great potential of activating H_2O_2. Meanwhile, some other active sites such as metal-complex and MoS_4^{2-} can be introduced into interlayer of LDH for H_2O_2 activation owing to the strong anion exchange capacity of LDH (Ali et al. 2020, Jawad et al. 2017, Wang et al. 2017). Bai et al. employed Co-Fe LDH for Fenton-like degradation of nitrobenzene, where Co(II)/Co(III) was possible to decomposing H_2O_2 to generate hydroxyl radical ($^{\bullet}OH$) (Bai et al. 2017). Similarly, CuMgFe LDH with CO_3^{2-} intercalation was prepared for Fenton-like degradation of sulfathiazole (de Melo Costa-Serge et al. 2021). However, the electrical conductivity of LDH is usually limited (Chen et al. 2021b, Ma et al. 2015, Zhao et al. 2012). As reported by Chen et al., the electrical conductivity of LDH was unsatisfactory owing to the its poor carrier mobilities and aggregation during formation process (Chen et al. 2021b). Zhao et al. also found that carbon nanotubes possessed a high electrical conductivity at 0.17-2 × 10^{-5} S/cm, while LDH was unconducive (Zhao et al. 2012). This will correspondingly reduce the electron transmission rate and slow down the reaction rate in LDH/H_2O_2 system.

Biochar (BC) is an attractive carbon material produced from various waste biomass, which exhibits great potential in environmental remediation owing to its low-cost, porous structure, as well as plentiful surface functional groups (Fang et al. 2014, Xin et al. 2021). It has been reported that BC could provide a large reactive area for the growth of metal catalysts, therefore reducing their aggregation (Peng et al. 2021, Yang et al. 2019a). Some researchers also indicated that combining with BC was capable of improving the electron transmission rate owing to its remarkable electrical conductivity and abundant redox-active moieties (i.e., carboxylic acid, quinoid C=O, and phenolic -OH) (Fang et al. 2021, Li et al. 2022c, Liu et al. 2020, Ye et al. 2021). For example, in the study of photocatalytic degrading tetracycline with ZnO/ZnFe-LDH/BC as catalyst, the photogenerated electron (e^-) effectively migrated to the BC surface, which could thus reduce the recombination rate of hole (h^+) and e^- (Li et al. 2022c). Liu et al. also reported that the carboxyl group on BC could complex with Fe in goethite, then the electrons would be shifted from bound Fe to the carbonyl group, and accelerate Fe(III)/Fe(II) redox cycle (Liu et al. 2020). As reported, BC with redox activity is capable of participating in the electronic interaction (Ye et al. 2021). Therefore, it is hypothesized that coupling of LDH with BC is a potential and suitable method to promote the H_2O_2 activation performance, not only owing to the improved electron transfer, but also the modulated electron distribution caused by the redox reaction between LDH and BC. However, the related literatures are rarely reported. The synergistic mechanism between LDH and BC in Fenton-like reaction deserves further investigations.

Therefore, we prepared the Cu-Co LDH/BC composite through a simple coprecipitation method in this study. Cu and Co are selected as fabrication agents of LDH owing to the following reasons: (i) both Cu and Co are widely used transition metal species for activating H_2O_2 (Chen et al. 2021a); (ii) Cu(I) can be oxidized by Co(III) thermodynamically according to their redox potential, this synergistic effect can promote the electron transfer in the reaction system (Wang et al. 2020b); and (iii) Cu and Co have been proven to be capable of synthesizing LDH because of their multi-valence and similar radius (Cu^{2+} (0.69 Å), Co^{2+}(0.74 Å), Co^{3+}(0.63 Å)) to that of Mg^{2+} (0.65 Å) (Li et al. 2015). The main purposes were to (i) study the catalytic activity of Cu-Co LDH/BC, and effects of different experimental conditions (i.e., H_2O_2 dosage and initial solution pH) on CIP degradation; (ii) elucidate the mechanism of H_2O_2 activation by Cu-Co LDH/BC and explore the synergistic effect of BC and Cu-Co LDH; and (iii) clarify the possible intermediate products and degradation pathway of CIP.

2. Materials and methods

2.1 Materials

The pine needles biomass was collected from Changsha of Hunan province, China. The sodium hydroxide (NaOH), sodium carbonate (Na_2CO_3), copper chloride dihydrate ($CuCl_2·2H_2O$), cobalt chloride hexahydrate ($CoCl_2·6H_2O$), L-tryptophan, Tert-butyl alcohol (TBA), 2,2,6,6-tetramethylpiperidine (TEMPOL), 1,3-diphenylisobenzofuran (DPBF), dimethyl sulfoxides (DMSO) and CIP were acquired from Sinopharm Chemical Reagent Corp (Beijing, China). Ultrapure water was used throughout the solution experiments, whose resistivity was determined to be 18.25 MΩ.

124 2.2 Preparation of catalysts

125 The preparation procedures for the BC referred to our previous studies (Lai et al.
126 2019, Li et al. 2019). Specifically, the collected biomass was firstly washed with
127 ultrapure water, then drying at 105 ℃. The achieved sample subsequently grinded
128 through a pulverizer, following by passing through a 100-mesh sieve to acquire pine
129 needle feedstock. For preparing pure BC, 8 g pine needle feedstock was pyrolyzed at
130 550 ℃ in the N_2 atmosphere for 2 h (heating rate of was set to be 10 ℃/min). The
131 obtained material was washed alternately with alcohol and ultrapure water, then drying
132 overnight at 60 ℃. When preparing Cu-Co LDH/BC composite, 0.2046 g $CuCl_2 \cdot 2H_2O$
133 and 0.0714 g $CoCl_2 \cdot 6H_2O$ (total amount of metal was 0.015 mol, and Cu/Co molar ratio
134 was 4:1) (Guo et al. 2020, Liu et al. 2010) were dissolved in 30 mL ultrapure water
135 containing 0.1 g BC, then Na_2CO_3/NaOH solution (C_{Na2CO3} =0.2 mol/L, C_{NaOH} = 0.4
136 mol/L) was added drop by drop through the peristaltic pump for adjusting solution pH
137 to 12. This obtained solution subsequently stirred at 65 ℃ for 24 h, following by
138 washing alternately with alcohol and ultrapure water. The achieved catalyst was then
139 dried overnight at 60 ℃ to acquire Cu-Co LDH/BC composite. For comparison, Cu-Co
140 LDH/BC(0.08), Cu-Co LDH/BC(0.2), and Cu-Co LDH/BC(0.3) was prepared by
141 adding the same amount of $CuCl_2 \cdot 2H_2O$ and $CoCl_2 \cdot 6H_2O$ into ultrapure water
142 containing 0.08 g, 0.2 g, and 0.3 g BC, respectively. Cu/BC and Co/BC was synthesized
143 with the same procedures as Cu-Co LDH/BC, and the dosage of $CuCl_2 \cdot 2H_2O$ and
144 $CoCl_2 \cdot 6H_2O$ was determined to be 0.015 mol, respectively. The Cu-Co LDH was
145 synthesized through the same steps without BC addition.

146 2.3 Characterization of catalysts

147 Transmission electron microscopy (TEM), Scanning electron microscope (SEM),
148 Energy-dispersive spectrometry (EDS)-elemental mapping, thermogravimetric analysis
149 (TGA), N_2 adsorption-desorption isotherms, Fourier transform infrared (FT-IR)
150 spectrophotometer, X-ray diffractometer (XRD), X-ray photoelectron spectrometry
151 (XPS), Electrochemical impedance spectroscopy (EIS), Liner Sweep Voltammetry
152 (LSV), and Chronoamperometry test have been employed to characterize the structure
153 properties of catalysts in this study. Text S1 provided the detailed information.

154 2.4 Catalytic experimental process

155 The catalytic experiments were all performed at room temperature without light
156 irradiation. Firstly, adsorption experiment was performed in a 200 mL breaker
157 containing 100 mL CIP and catalyst to study the adsorption characteristics of prepared
158 catalysts. CIP concentration was decided to be 10 mg/L according to the concentration
159 of CIP in actual wastewater and other works relating to CIP degradation (Table S1). As
160 shown in Fig. S1, the adsorption of CIP reached equilibrium within 30 min in all three
161 studied systems. Based on this result, in a typical degradation experiment, the
162 suspension (100 mL) containing CIP (10 mg/L) and catalyst was primarily stirred to
163 obtain the adsorption/desorption equilibrium. After stirring for 30 min, the catalytic
164 reaction was then triggered by injecting a certain volume of H_2O_2. During catalytic
165 reaction, samples were taken at a regular time, 0.45 μm Millipore membrane filter was
166 used to filtrated the solution. The solution was subsequently quenched with 70 μL TBA
167 for further analysis. To study the reusability of catalyst, the sample after catalytic

168 reaction was centrifuged, washed alternatively with deionized water and ethanol, and
169 eventually dried at 60 ℃. The obtained catalyst was collected for reuse.
170 2.5 Analytic methods
171 A Shimadzu UV-vis spectrophotometer was used to analyze the concentration of
172 CIP, and the maximum absorbance wavelength was measured to be 276 nm. The signals
173 of reactive species including $^{\bullet}OH$, superoxide radical ($O_2^{\bullet-}$), and singlet oxygen ($^1O_2$)
174 were identified by Electron spin resonance (ESR) technology with DMPO and TEMP
175 as spin-trap reagent, respectively. The total organic carbon (TOC) removal efficiency
176 was studied through Shimadzu TOC-VCPH analyzer. The leached concentration of Cu
177 and Co was identified by inductively coupled plasma mass spectrometry (ICP-MS,
178 Agilent 7900). The intermediate products of CIP were investigated by through a high-
179 performance liquid chromatography-mass spectrometry (HPLC-MS, 1290/6460 Triple
180 Quad) equipped with a C18 chromatographic column (5 μm, 250 mm × 3.5 mm), the
181 detailed detecting condition was described as follows: the isocratic mobile phase was
182 prepared by using 0.1% formic acid and methyl alcohol with the ratio of 70:30 (v/v),
183 and the flow rate was set to be 0.2 mL/min.
184 **3. Results and discussion**
185 3.1 Catalysts characterization
186 Firstly, TGA was employed to study the eventual loading rate of Cu-Co LDH on
187 BC. For the TGA curvy of Cu-Co LDH (Fig. S2), the weight loss at approximate 20℃-
188 200℃ can be ascribed to the loss of interlayer and adsorbed water, and further increase
189 of temperature would lead to the dihydroxylation of layers as well as removal of

190 interlayer CO_3^{2-} (Li et al. 2015). Meanwhile, the pure BC was completely decomposed
191 when raising temperature to 800°C. In comparison, about 46.8% of Cu-Co LDH/BC
192 remained. Therefore, the eventual loading rate of Cu-Co LDH on BC can be studied via
193 weight remainder, which was determined to be 60%.

194 Then, the morphology of Cu-Co LDH, BC, and Cu-Co LDH/BC were studied
195 through SEM and TEM technology. It can be observed from Fig. 1(A) that the Cu-Co
196 LDH consisted of irregular layered structure with a plate-like shape folded, which was
197 in accordance with the typical morphology of LDH. Also, the images in Fig. 1(B)
198 revealed that the pure BC possessed a relatively smooth surface with some micro-pores
199 existing on it. In comparison, the surface of Cu-Co LDH/BC was much rougher (Fig.
200 1(C-D)) with many irregular flake crystals distributing uniformly on the surface of Cu-
201 Co LDH/BC. Then EDS-elemental manning (Fig. 1(E)) was employed to investigate
202 the composition distribution of Cu-Co LDH/BC, which revealed the uniform
203 distribution of C, Co, Cu, and O. Furthermore, the EDS spectrum (Fig. S3) of Cu-Co
204 LDH/BC showed that the Cu/Co atomic ratio was about 4.43, which was closely to the
205 theoretical value of Cu-Co LDH/BC. As for TEM images, the results in Fig. 1(F)
206 indicated the presence of dual material morphology and formation of a composite
207 hybrid. Moreover, the high-resolution TEM image of Cu-Co LDH/BC (Fig. 1(G-H))
208 showed the lattice fringes of 0.261 for the (012) planes of Cu-Co LDH (Lu et al. 2019),
209 further verifying the successful loading of Cu-Co LDH onto BC surface.

210 N_2 adsorption-desorption isotherms were then applied to study the surface area
211 and pore characteristic of Cu-Co LDH, BC, and Cu-Co LDH/BC by using BET and

BJH methods, respectively. As presented in Table 1 and Fig. S4, the BET surface area of Cu-Co LDH, BC and Cu-Co LDH/BC were 70.075 m^2/g, 3.579 m^2/g, and 87.537 m^2/g respectively, the average pore diameters were 4.272 nm, 4.286 nm, and 3.439 nm, respectively, and the pore volume were 0.357 cm^3/g, 0.015 cm^3/g, and 0.269 cm^3/g, respectively. The increased surface area of Cu-Co LDH/BC compared with Cu-Co LDH may be ascribed to the more uniform distribution of Cu-Co LDH over BC surface. In general, catalyst possessing larger surface area could expose more reaction sites for substrate contact, which was conductive to improve the catalytic performance.

The crystal structures of BC, Cu-Co LDH, and Cu-Co LDH/BC were indicated through XRD analysis. As observed from Fig. 2(A), Cu-Co LDH exhibited characteristic diffraction peaks at $2\theta = 23.8°$, 34.4°, and 39.6°, representing the typical (006), (012), and (015) crystal planes of LDH, respectively (JCPDS: 40-0215) (Khataee et al. 2019, Yang et al. 2019b). Besides, the diffraction peaks at $2\theta = 16.6°$ and 35.8° could be indexed to $Cu(OH)_2$ (JCPDS: 45-0594) (Guo et al. 2020), and the other peak at $2\theta = 53.5°$ could be referred to $Co(OH)_2$ (JCPDS: 78-2177) (Liu et al. 2010). Regarding for pure BC, a broad diffraction peak at approximately 23° corresponded to the (002) plane of graphitic structure of BC (Zhou et al. 2020). Nevertheless, for Cu-Co LDH/BC, the characteristic peaks of Cu-Co LDH were observed, but no obvious peak of BC was found. This may be because the peak position of (002) plane of BC was closely to that of (006) plane of Cu-Co LDH, therefore, the characteristic peak of biochar could not be clearly observed in the XRD pattern of Cu-Co LDH/BC. This conclusion could be verified by the XRD pattern of Cu-Co LDH/BC after reaction at

pH 3.0 (Fig. S5(A)), where almost all peaks corresponding to the Cu-Co LDH was disappeared owing to the damage of structure, and a broad diffraction peak relating to the (002) plane of graphitic structure of BC was then found. Meanwhile, the interlayer spacing of Cu-Co LDH was determined to be 0.373 nm, and that of Cu-Co LDH/BC was determined to be 0.368 nm from the position of (006) reflection based on Braggs equation ($d = n\lambda/2\sin\theta$, $\lambda = 0.154$), and the average particle size of Cu-Co LDH and Cu-Co LDH/BC was calculated to be 7.53 nm and 6.2 nm respectively according to Scherrer equation ($D= k\lambda/w\cos\theta$, $k = 0.89$). This indicated that BC can effectively reduce the aggregation of LDH. The above results further indicated the successfully synthesis of Cu-Co LDH/BC composite.

The surface functional groups of Cu-Co LDH, BC, and Cu-Co LDH/BC were subsequently determined through FTIR analysis (Fig. 2(B)). As for Cu-Co LDH, the peak at 3576 cm^{-1} corresponded to the O-H stretching vibration of $Cu(OH)_2$ (Guo et al. 2020), and the peak at approximately 3311 cm^{-1} was ascribed to the O-H stretching, which can be explained by the existence of interlayer and adsorbed water and hydroxyl groups. Meanwhile, a peak at 1630 cm^{-1} belonged to the H-O-H bending vibration (Gholami et al. 2020, Jiang et al. 2021). The stretching and bending vibration of CO_3^{2-} displayed at the peaks of 1387 cm^{-1} and 695 cm^{-1}, respectively (Tian et al. 2019). Additionally, the peaks observed from 400-500 cm^{-1} were assigned to the M-O vibrations (M = Cu or Co). For Cu-Co LDH/BC, in addition to these peaks, the other peaks located at 872 cm^{-1}, 1448 cm^{-1}, and 1580 cm^{-1} can be attributed to aromatic C-H, -COOH, as well as well as C=C/C=O groups of BC, respectively (Li et al. 2019, Li et

al. 2021a). Meanwhile, it was noticed that the stretching band of -OH (from 3424 to 3311 cm^{-1}), -COOH (from 1426 to 1448 cm^{-1}) and C=C/C=O (from 1600 cm^{-1} to 1580 cm^{-1}) in Cu-Co LDH/BC had a slight shift in comparison with pure BC. This might be because the interaction between Cu-Co LDH and these functional groups of BC altered the chemical environment of functional groups, thereby resulting in the shift of stretching band (Xin et al. 2021).

Besides, EIS and LSV tests were employed to investigate the electron transfer capacity of Cu-Co LDH and Cu-Co LDH/BC. For the EIS results, an equivalent circuit containing solution resistance (R_s), charge transfer resistance (R_{ct}), Warburg impedance (W_o), and interfacial capacitance (C_{dl}) was used to fit the data, and R_{ct} (diameter of the arc) was usually employed to estimate the electron transfer capacity (Lai et al. 2018, Zhou et al. 2020). As presented in Fig. 2(C), Cu-Co LDH showed a larger R_{ct} of 6835 Ω, and Cu-Co LDH/BC showed a smaller R_{ct} of 4740 Ω. In general, a smaller R_{ct} represented a stronger ability for electron transfer. Therefore, Cu-Co LDH/BC was considered to have better electron conductivity. This conclusion was further confirmed by LSV results. As seen from Fig. 2(D), Cu-Co LDH/BC/H_2O_2 system showed stronger current response than Cu-Co LDH/H_2O_2 system. This demonstrated that the electron transfer process was accelerated in Cu-Co LDH/BC/H_2O_2 system, which may be beneficial for the Fenton-like catalytic process.

Then, the element composition and element valence of catalysts were investigated by XPS measurement with the results presenting in Table S2 and Fig. 3. The full XPS survey of Cu-Co LDH/BC (Fig. 3(A)) indicated the existence of Co, Cu, C, and O

elements. Besides, Fig. 3(B) showed the high-resolution XPS spectra of Cu 2p, and Fig. 3(C) showed that of Co 2p. For Cu-Co LDH, the Cu 2p XPS spectra was deconvoluted into five types of peaks. The peak with binding energy of 935.3 eV belonged to the Cu $2p_{3/2}$, and the peak at 955.2 eV was attributed to the Cu $2p_{1/2}$, both of them verified the existence of Cu(II) in Cu-Co LDH (Cheng et al. 2019). Besides, the peaks at 942.4 eV and 944.5 eV can be ascribed to the signals for the satellite peaks for Cu $2p_{3/2}$, and the peak at 963.0 eV belonged to the satellite peak for Cu $2p_{1/2}$ (Pan et al. 2021). Meanwhile, as seen from Fig. 3(C), the Co 2p spectra of Cu-Co LDH were well-fitted into six peaks, in which two prominent peaks with binding energy of 781.1 eV and 796.6 eV referred to the Co $2p_{3/2}$ and Co $2p_{1/2}$ of Co(III) oxidation state, respectively (Wang et al. 2020b). The peaks for Co(II) oxidation state were found at 782.0 eV and 797.9 eV (Hong et al. 2021). Furthermore, the other two peaks located at 785.7 eV and 803.2 eV were the signals of satellite peaks for Co(III) (Long et al. 2017). Compared with Cu-Co LDH, the Cu 2p and Co 2p spectra in Cu-Co LDH/BC shifted towards higher binding energy. As previous reported, the variation of electron density could be reflected by the shift of binding energy position in XPS spectra. The shift towards higher value was because of the weakened electron shielding effect arisen from the reduction of electron concentration, conversely, the shift towards lower value meant the increase of electron concentration (Feng et al. 2021, Yang et al. 2019b). Therefore, the increase of binding energy of Cu 2p and Co 2p XPS spectra may be related to reduced electron density of Cu and Co in Cu-Co LDH/BC. As some previous literatures reported, some oxygen-containing functional groups of BC (i.e., -COOH and quinone C=O) was capable of

accepting electrons during reaction, thereby affecting the electron distribution (Sathishkumar et al. 2020, Yuan et al. 2018). Moreover, from Table S2, it was found that the peak area ratio of Co(III) in Cu-Co LDH/BC (48.5%) was higher than that in Cu-Co LDH (35.2%), demonstrating that more Co(III) was existed in Cu-Co LDH/BC, which further confirmed the electronic interaction during synthesizing Cu-Co LDH/BC composite. These results were consistent with those in FTIR analysis.

Besides, the XPS spectra of Cu-Co LDH/BC after reaction was also presented in Fig. 3. Fig. 3(B) showed the high-resolution XPS spectra of Cu 2p, and Fig. 3(C) showed that of Co 2p, all these peaks had a shift towards lower binding energy after Fenton-like reaction. This might be ascribed to the increased electron concentration around Cu and Co, which could lead to the partial reduction of Cu(II) and Co(III) to Cu(I) and Co(II). Meanwhile, the peak area ratio of Co(III) decreased from 48.5% to 45.2%, and the peak area ratio of Co(II) increased from 51.5% to 54.8% after Fenton-like reaction, further verified the conversion of Co(III) to Co(II). However, no peaks corresponding to Cu(I) were found in Cu 2p XPS spectrum of Cu-Co LDH/BC after reaction, which may be because the Cu(I) existed inside the catalysts could not be detected by XPS characterization (Du et al. 2018), or the oxidation of Cu(I) by Co(III) (Eqs. (1)-(3)) (Wang et al. 2020b).

As for C 1s XPS spectrum of Cu-Co LDH/BC before reaction (Fig. 3(D)), it can be deconvoluted into four peaks including C=C at 284.8 eV, C-C at 285.9 eV, C-OH at 287.4 eV, and O-C=O at 289.4 eV (He et al. 2020, Li et al. 2021a). After Fenton-like reaction, the peak area radio of C=C decreased from 52% to 31%, and that of C-C

322 decreased from 29.4% to 21.3%. Conversely, the peak area radio of C-O increased from
323 3.3% to 20.7%, and that of C=O increased from 15.3% to 27% (Table S2). It has been
324 widely reported that C=C of BC was able to activate H_2O_2 to generate •OH via single-
325 electron transfer (Luo et al. 2019). However, in this study, the BC/H_2O_2 system can
326 hardly degrade CIP. It is thus speculated that the free-flowing π-electron from C=C
327 mainly promoted the nearby metal redox cycle (Co(III)/Co(II) and Cu(II)/Cu(I)), rather
328 than activating H_2O_2 in this study.

$$Co(III) + e^- \rightarrow Co(II) \quad (E^0 = 1.81V) \tag{1}$$

$$Cu(II) + e^- \rightarrow Cu(I) \quad (E^0 = 0.17V) \tag{2}$$

$$Co(III) + Cu(I) \rightarrow Co(II) + Cu(II) \tag{3}$$

329

330 Overall, combining Cu-Co LDH with BC was possible to enhance the surface area,
331 increase the oxygen-containing functional groups, affect the charge distribution, and
332 promote electron transfer. All of these synergistic effects were expected to endow Cu-
333 Co LDH/BC with better Fenton-like catalytic activity.

334 3.2 Catalytic performance testing

335 The results of CIP degradation were applied to evaluate the Fenton-like catalytic
336 activity of prepared catalysts. It can be observed from Fig. 4(A) that CIP concentration
337 barely reduced in H_2O_2 solution without catalyst, indicating that H_2O_2 alone could
338 hardly degrade CIP. Besides, when BC and H_2O_2 were used together, the CIP
339 concentration only decreased by 23.6%, which demonstrated that pure BC cannot
340 effectively active H_2O_2 to degrade CIP. Meanwhile, both Cu/BC/H_2O_2 system and
341 Co/BC/H_2O_2 system cannot effectively degrade CIP, illustrating the important role of

synergistic effect between Cu and CO and unique structure of LDH. In comparison, the CIP degradation efficiency in Cu-Co LDH/H_2O_2, Cu-Co LDH/BC(0.08)/H_2O_2, Cu-Co LDH/BC/H_2O_2, Cu-Co LDH/BC(0.2)/H_2O_2, and Cu-Co LDH/BC(0.3)/H_2O_2 systems was 72%, 59.2%, 84.7%, 71.5%, and 65.8%, respectively (Fig. S6). The lower degradation efficiency in Cu-Co LDH/BC(0.08)/H_2O_2 may be ascribed to the agglomeration of excessive Cu-Co LDH, and the lower degradation efficiency in Cu-Co LDH/BC(0.2)/H_2O_2 as well as Cu-Co LDH/BC(0.3)/H_2O_2 systems may be because more BC hindered the active sites over Cu-Co LDH from reacting with H_2O_2. Therefore, Cu-Co LDH/BC/H_2O_2 was utilized in the subsequent experiments. Meanwhile, the pseudo-first-order kinetic fitting curve (after adsorption equilibrium) showed that the rate constant of Cu-Co LDH/BC/H_2O_2 system (k = 0.05 min^{-1}) was approximately 1.5 times than that of Cu-Co LDH/H_2O_2 system (k = 0.02 min^{-1}) (Fig. 4(B)), further verifying the better catalytic activity of Cu-Co LDH/BC. Besides, the physical mixing system of Cu-Co LDH and BC was also employed for CIP degradation, and the dosage of Cu-Co LDH was determined by the eventual loading rate of Cu-Co LDH over Cu-Co LDH/BC. As seen from Fig. 4(A), the CIP degradation efficiency in this physical mixing system (approximately 52%) was much lower than that in Cu-Co LDH/BC/H_2O_2 system, which confirmed the important role of synergistic effects between BC and LDH in improving catalytic activity.

Besides, the degradation efficiency at different catalyst dosage was also studied. The results in Fig. 4(C) indicated that the degradation efficiency of CIP was 40.6%, 84.7%, and 83.5% at catalyst dosage of 100 mg/L, 200 mg/L, and 300 mg/L,

364 respectively. The increase of catalyst dosage was capable of providing more active sites
365 for activating H_2O_2 to degrade CIP, but the excess catalyst may result in the scavenge
366 of generated reactive species (Li et al. 2019, Wang et al. 2020c). Therefore, 200 mg/L
367 was utilized in this study.

368 Then, the degradation of CIP at different H_2O_2 dosage was investigated since H_2O_2
369 is the direct driving force related to contaminant degradation in Fenton-like reaction, it
370 is thus significant to add appropriate H_2O_2 dosage. The results in Fig. 4(D)
371 demonstrated that when increasing H_2O_2 dosage from 5 mmol/L to 20 mmol/L, CIP
372 degradation efficiency increased from 29.7% to 84.7%, this may be because H_2O_2 could
373 be activated by the abundant active sites on Cu-Co LDH/BC surface and generate more
374 reactive species for CIP degradation. However, when further increasing H_2O_2 dosage
375 from 20 mmol/L to 30 mmol/L, the degradation efficiency of CIP decreased from 84.7%
376 to 79.5%. It may be that the excessive H_2O_2 would quench the generated $\bullet OH$,
377 therefore lowering the CIP degradation efficiency (Cheng et al. 2019, Wang et al.
378 2020c). As a result, the optimal dosage of H_2O_2 was 20 mmol/L, which was utilized in
379 subsequent experiments.

380 The effects of solution pH on CIP degradation in Cu-Co LDH/BC/H_2O_2 system
381 was further investigated since the catalytic activity of Fenton-like reaction was highly
382 dependent on solution pH. As for CIP solution, the initial pH was determined to be 5.4,
383 and the other solution pH were adjusted by adding certain amount of NaOH and HCl.
384 As displayed in Fig. 4(E), Cu-Co LDH/BC maintained high catalytic activity at pH 4.5
385 to 8.9, and Cu-Co LDH/BC exhibited relatively high degradation efficiency to CIP at

386 neutral initial pH. However, the degradation efficacy of CIP decreased to 56.8% when
387 adjusting solution pH to 3.0, which may be because of the destruction of hydroxide
388 layer of LDH by H^+ (Deng et al. 2021). In order to verify this speculation, the XRD
389 pattern of Cu-Co LDH/BC after reaction at pH 3.0 were measured. Not surprising, the
390 results in Fig. S5(A) suggested that the characterization peaks almost disappeared after
391 reaction at pH 3.0, indicating the damage of structure. Meanwhile, more leaching
392 concentration of Cu and Co could be observed at pH 3.0 (Fig. S7), which would lead to
393 the decrease of active sites over Cu-Co LDH/BC. Besides, CIP degradation efficiency
394 decreased to 59.8% at pH 11.0, this was probably because of the accelerated
395 decomposition of H_2O_2 to H_2O and O_2 in a strong alkaline solution (Lai et al. 2019).
396 Then, the variation of solution pH during catalytic process were studied to better
397 understand the influence of solution pH on this Fenton-like process. It is interesting to
398 find that the pH variation was basically consistent with the trend of CIP degradation
399 (Fig. S5(B)). After adsorption, the solution pH changed from 4.5, 7.0, and 8.9 to 7.1,
400 7.3, and 7.6 respectively, and had little change in the subsequent degradation process.
401 However, the solution pH decreased to 10.85 after adsorption when the initial pH was
402 11.0, which was not conductive to the proceeding of Fenton-like reaction. Besides,
403 although the pH increased from initial 3.0 to 5.99 after adsorption process, the
404 degradation efficiency of CIP was still unsatisfactory at pH 3.0, which was due to the
405 destruction of hydroxide layer of LDH. In addition, the CIP degradation in Cu-Co
406 LDH/H_2O_2 system at various solution pH were also studied for comparison (Fig. 4(F)).
407 It can be observed that the CIP degradation efficiency was determined to be 16.3%,

67.2%, 72%, 76.6%, 51%, and 36.8% respectively at pH 3.0, 4.5, 5.4, 7.0, 8.9, and 11.0. Obviously, Cu-Co LDH/BC/H_2O_2 system achieved better catalytic performance at a wider range of pH, which may be because the abundant functional groups on BC surface could react with H^+ or OH^- to buffer pH variation.

3.3 Mechanistic study in Cu-Co LDH/BC system

3.3.1 The contribution of radical pathway

The main free radicals in Cu-Co LDH/BC/H_2O_2 system were firstly identified by ESR technology with the results presenting in Fig. 5. From Fig. 5(A-B), the strong signals assigned to DMPO-$^{\bullet}$OH, and DMPO-$O_2^{\bullet-}$ could be detected, and the signals intensities enhanced with reaction time increasing, indicating the production of $^{\bullet}$OH, and $O_2^{\bullet-}$ in Cu-Co LDH/BC/H_2O_2 system. Furthermore, so as to study the contribution of different ROS in Cu-Co LDH/BC/H_2O_2 system, the quenching experiments were conducted with TEMPOL and TBA as the scavenger of $O_2^{\bullet-}$ and $^{\bullet}$OH, respectively. It was surprisingly found that the degradation efficacy of CIP slightly reduced after addition of TBA (Fig. 5(C)), suggesting that $^{\bullet}$OH played a minor role in Cu-Co LDH/BC/H_2O_2 system. Meanwhile, the presence of TEMPOL decreased the degradation efficiency of CIP from 84.7% to 30.2%, manifesting that $O_2^{\bullet-}$ was primarily contributed to the degradation of CIP in Cu-Co LDH/BC/H_2O_2 system. Then, in order to identify the separated contribution of Cu-Co LDH and BC during catalytic reaction, the free radical quenching experiments were conducted in Cu-Co LDH/H_2O_2 system and BC/H_2O_2 system with addition of same dose of TBA and TEMPOL. As seen from Fig. 5 (D), there was no obvious distinction in CIP degradation in BC/H_2O_2 and

430 BC/H_2O_2/quencher systems. For Cu-Co LDH/H_2O_2 system, the presence of TBA and
431 TEMPOL decreased the degradation efficacy from 72% to 63.6% and 52.5%,
432 respectively. By comparison, it can be found that the inhibitory effect of TEMPOL on
433 $O_2^{\bullet-}$ was more prominent in Cu-Co LDH/BC/H_2O_2 system. This may be because the
434 electronic interaction between Cu-Co LDH and BC resulted in the presence of more
435 Co(III) and Cu(II) over Cu-Co LDH/BC surface, seen from XPS analysis. Then, the
436 generated Co(III) and Cu(II) activated H_2O_2 to produce $O_2^{\bullet-}$ through Eqs. (4-6).

$$Cu(II) + H_2O_2 \rightarrow Cu(I) + HO_2\cdot + H^+ \quad (4)$$

$$Co(III) + H_2O_2 \rightarrow Co(II) + HO_2\cdot + H^+ \quad (5)$$

$$HO_2\cdot \rightleftharpoons \cdot O_2^- + H^+ \quad (6)$$

437

438 3.3.2 The contribution of nonradical pathway

439 In addition to free radicals, it has been widely reported that some nonradical
440 pathway such as $^1O_2$, mediated electron transfer from contaminants to H_2O_2, and high-
441 valent metal species may also contribute to contaminants degradation during Fenton-
442 like reaction (Chen et al. 2021a, Li et al. 2021b, Zhuang et al. 2019). Therefore, the role
443 of nonradical pathway were also investigated in this study.

444 To be specific, L-Tryptophan was employed as the scavenger to explore the
445 contribution of $^1O_2$. The result (Fig. 5(C)) indicated that with the addition of L-
446 Tryptophan, the degradation efficiency of CIP decreased by almost 30%, manifesting
447 that $^1O_2$ played an important role for CIP degradation in Cu-Co LDH/BC/H_2O_2 system.
448 The TEMP-$^1O_2$ signal in ESR results also demonstrated the existence of $^1O_2$ (Fig. 5(E)).
449 Meanwhile, the same dose of L-Tryptophan decreased the CIP degradation efficiency

by about 14.5% in Cu-Co LDH/H_2O_2 system (Fig. 5(D)), and the inhibitory effect was not as obvious as that in Cu-Co LDH/BC/H_2O_2 system. For investigating the possible reasons, the DPBF degradation experiments with TBA and TEMPOL as scavengers were firstly conducted to investigate the formation path of $^1O_2$ in Cu-Co LDH/BC/H_2O_2 system since DPBF can be used as the $^1O_2$ trapping agent (Zhang et al. 2020, Zhao and Zhao 2019). The results were presented in Fig. 6(F). As observed, the degradation efficacy of DPBF in Cu-Co LDH/BC/H_2O_2 system was closely to that in Cu-Co LDH/BC/H_2O_2/TBA system, while DPBF slightly degraded in the presence of TEMPOL. This suggested that the $O_2^{\bullet-}$ conversion was responsible for $^1O_2$ formation. As previous literatures reported, the direct recombination of $O_2^{\bullet-}$ and $HO_2^{\bullet}$ (Eqs. (7-8)) would lead to the generation of $^1O_2$ (Li et al. 2021b, Nosaka and Nosaka 2017). Therefore, the presence of more $O_2^{\bullet-}$ in Cu-Co LDH/BC/H_2O_2 system may be responsible for the enhanced $^1O_2$ generations.

$$\cdot O_2^- + HO_2\cdot + H^+ \rightarrow {}^1O_2 + H_2O_2 \quad (7)$$

$$2\cdot O_2^- + 2H_2O \rightarrow {}^1O_2 + H_2O_2 + 2OH^- \quad (8)$$

Furthermore, for studying the contribution of electron transfer pathway in the Cu-Co LDH/BC/H_2O_2 system, chronoamperometry curves was recorded to track current response during reaction. It can be observed from Fig. S8 that CIP injection only resulted in a weak current spike, and the current intensity significantly increased after subsequent H_2O_2 addition. More importantly, little distinction can be observed from the current intensity of Cu-Co LDH/BC/CIP/H_2O_2 system and Cu-Co LDH/BC/H_2O_2 system. It can be thus speculated that electron-transfer induced non-radical pathway

471 was not the major contribution for CIP degradation in Cu-Co LDH/BC/H_2O_2 system.

472 In addition, the role of in-situ formed high valence metal in CIP degradation was
473 investigated by using DMSO as a quencher. The results (Fig. 5(C)) demonstrated that
474 the degradation efficacy of CIP slightly decreased to 80.3% in response to DMSO
475 addition, which indicated that in-situ formed high valence metal played a minor role in
476 this study.

477 3.3.3 The possible reaction mechanism

478 Based on above analysis, a possible activation mechanism in Cu-Co
479 LDH/BC/H_2O_2 system was proposed as Fig. 6. In general, both homogeneous Fenton-
480 like reactions induced by leached Cu and Co in solution and heterogeneous Fenton-like
481 reactions occurred on Cu-Co LDH/BC surface would contribute to the CIP degradation.
482 The homogeneous reactions usually exhibited better catalytic performance under acidic
483 condition, therefore, the decrease of CIP degradation under acidic pH and effective CIP
484 degradation under neutral and basic pH all indicated that heterogeneous reactions
485 played a dominant contribution in this Cu-Co LDH/BC/H_2O_2 system. To be specific,
486 Cu-Co LDH/BC mainly containing Cu(II)/Co(III) would react with H_2O_2 via Eqs. (4-
487 5) to generate Cu(I)/Co(II) and $HO_2^{\bullet}$. Subsequently, Cu(I)/Co(II) activated H_2O_2 to
488 generate $^{\bullet}OH$ (Eqs. (9-10)), and the unstable $HO_2^{\bullet}$ could be quickly transferred into $O_2^{\bullet-}$
489 through Eq. 6. The generated $O_2^{\bullet-}$ could then recombine with itself or $HO_2^{\bullet}$ to form $^1O_2$
490 (Eqs. (7-8)). Meanwhile, the presence of BC served as electrons carrier and promoted
491 the electron transfer. In addition, the free-flowing π-electron from C=C and synergistic
492 effect between Cu and Co (Eqs. (1-3)) was possible to promote rate-limiting metal

493 redox cycle (Co(III)/Co(II) and Cu(II)/Cu(I) cycle), therefore accelerating the
494 production of reactive species. Finally, the produced reactive species were all involved
495 in the degradation of CIP.

$$Cu(I) + H_2O_2 \rightarrow Cu(II) + \cdot OH + OH^- \quad (9)$$

496 $$Co(II) + H_2O_2 \rightarrow Co(III) + \cdot OH + OH^- \quad (10)$$

497 3.4 Application potential in real water and reusability

498 Considering the practical application, the catalytic activity of Cu-Co LDH/BC was
499 also tested in real wastewater containing various organic/inorganic contaminants, and
500 the local Taozi lake as well as Xiangjiang river were chosen as the water sample. The
501 results (Fig. 7(A)) indicated that 76.6% of CIP was degraded in lake water, and 75.4%
502 of CIP was degraded in river water. The decrease of degradation performance could be
503 attributed to the competitive consumption of reactive species by inorganic ions or
504 organic contaminants in the water environment. Overall, this Cu-Co LDH/BC/H_2O_2
505 system was possible to remove most CIP in actual wastewater, which exhibited good
506 potential in real application.

507 To further investigate the reusability of catalyst, four successive experiments were
508 carried out at neutral initial pH. As displayed in Fig. 7(C), the degradation efficiency of
509 CIP gradually decreased with proceeding of consecutive experiments (from initial 84.7%
510 to 62.9%). This might be due to the following reasons: i) the leaching amount of Co
511 and Cu after first cycle was measured to be 4.743 and 0.099 mg/L respectively by ICP-
512 MS. Thus, the loss of Cu and Co would lead to the reduce of active sites; ii) some
513 residual by-products might block the catalytic active sites over catalyst, therefore

hindering the degradation of CIP. Besides, no apparent changes were found from the XRD pattern of Co-Cu LDH/BC before and after reaction (Fig. 7(B)), this further verified the stability of catalyst.

3.5 Identification of intermediate products and toxicity analysis

The intermediate products of CIP during Fenton-like reaction were further investigated by HPLC-MS, and Fig. S9 provided the detailed LC-MS spectra. The possible degradation pathways of CIP were then proposed (Fig. S10) based on these intermediate products and relevant literatures, and the discussions were presented in Text S2.

Besides, the seed germination experiment was also performed to study the environmental risk of these degradation intermediates. The operating procedures were displayed in Text S3, and the results were presented in Fig. S11. It can be found that compared with the blank group, the water sample containing degradation intermediates had little limitation on the germination percentage, indicating that the degradation intermediates had less toxicity.

4. Conclusion

In this work, Cu-Co LDH/BC composite was prepared through coprecipitation process. The combination with BC can not only enhanced the surface area, increased oxygen-containing functional groups, and promoted electron transfer, but also affected the charge distribution owing to the electronic interaction between Cu-Co LDH and BC, these characteristics endowed Cu-Co LDH/BC with considerable H_2O_2 activation efficiency for CIP degradation. The prepared Cu-Co LDH/BC also exhibited a

536 remarkable buffering capacity at pH 4.5-8.9, which could realize the efficient
537 degradation of CIP under a wider range of pH. Meanwhile, during the Fenton-like
538 process, Co(III)/Co(II) and Cu(II)/Cu(I) were mainly responsible for H_2O_2 activation
539 and $^{\bullet}OH$, $O_2^{\bullet-}$ and $^1O_2$ generation, in which $O_2^{\bullet-}$ and $^1O_2$ were primarily contributed to
540 the CIP degradation. These findings may bring a valuable insight into modulating the
541 Fenton-like mechanism.

542 **Acknowledgments**

543 This study was financially supported by the Program for the National Natural Science
544 Foundation of China (U20A20323, 51521006, 51779090, 52170161, 51879101,
545 51579098, 51709101, 51809090, 51909084), the National Program for Support of Top–
546 Notch Young Professionals of China (2014), the Program for Changjiang Scholars and
547 Innovative Research Team in University (IRT_13R17), and Hunan Natural Science
548 Foundation (2020JJ3009), Hunan Researcher Award Program (2020RC3025), Hunan
549 Provincial Science and Technology Plan Project (2018SK20410, 2017SK2243,
550 2016RS3026), the Fundamental Research Funds for the Central Universities
551 (531118010247, 531118040083), and the Science and Technology Innovation Program
552 of Hunan Province (2021RC2057).

553 **Reference**

554 Ali, J., Wenli, L., Shahzad, A., Ifthikar, J., Aregay, G.G., Shahib, I.I., Elkhlifi, Z., Chen,
555 Z. and Chen, Z. (2020) Regulating the redox centers of Fe through the enrichment
556 of Mo moiety for persulfate activation: A new strategy to achieve maximum
557 persulfate utilization efficiency. Water Res. 181, 115862.
558 Bai, J., Liu, Y., Yin, X., Duan, H. and Ma, J. (2017) Efficient removal of nitrobenzene
559 by Fenton-like process with Co-Fe layered double hydroxide. Appl. Surf. Sci. 416,
560 45-50.
561 Chen, F., Wu, X.-L., Shi, C., Lin, H., Chen, J., Shi, Y., Wang, S. and Duan, X. (2021a)
562 Molecular engineering toward pyrrolic N-rich M-N_4 (M = Cr, Mn, Fe, Co, Cu)
563 single-atom sites for enhanced heterogeneous Fenton-like reaction. Adv. Funct.
564 Mater. 31(13), 2007877.
565 Chen, Y., Yao, H., Kong, F., Tian, K., Meng, G., Wang, S., Mao, X., Cui, X., Hou, X.
566 and Shi, J. (2021b) V_2C MXene synergistically coupling FeNi LDH nanosheets
567 for boosting oxygen evolution reaction. Appl. Catal. B: Environ. 297, 120474.
568 Cheng, M., Liu, Y., Huang, D., Lai, C., Zeng, G., Huang, J., Liu, Z., Zhang, C., Zhou,
569 C., Qin, L., Xiong, W., Yi, H. and Yang, Y. (2019) Prussian blue analogue derived
570 magnetic Cu-Fe oxide as a recyclable photo-Fenton catalyst for the efficient
571 removal of sulfamethazine at near neutral pH values. Chem. Eng. J. 362, 865-876.
572 de Melo Costa-Serge, N., Gonçalves, R.G.L., Rojas-Mantilla, H.D., Santilli, C.V.,
573 Hammer, P. and Nogueira, R.F.P. (2021) Fenton-like degradation of sulfathiazole
574 using copper-modified MgFe-CO_3 layered double hydroxide. J. Hazard. Mater.

413, 125388.

Deng, J., Xiao, L., Yuan, S., Wang, W., Zhan, X. and Hu, Z.-H. (2021) Activation of peroxymonosulfate by CoFeNi layered double hydroxide/graphene oxide (LDH/GO) for the degradation of gatifloxacin. Sep. Purif. Technol. 255, 117685.

Du, X., Li, C., Zhao, L., Zhang, J., Gao, L., Sheng, J., Yi, Y., Chen, J. and Zeng, G. (2018) Promotional removal of HCHO from simulated flue gas over Mn-Fe oxides modified activated coke. Appl. Catal. B: Environ. 232, 37-48.

Fang, G., Gao, J., Liu, C., Dionysiou, D.D., Wang, Y. and Zhou, D. (2014) Key role of persistent free radicals in hydrogen peroxide activation by biochar: Implications to organic contaminant degradation. Environ. Sci. Technol. 48(3), 1902-1910.

Fang, Q., Ye, S., Yang, H., Yang, K., Zhou, J., Gao, Y., Lin, Q., Tan, X. and Yang, Z. (2021) Application of layered double hydroxide-biochar composites in wastewater treatment: Recent trends, modification strategies, and outlook. J. Hazard. Mater. 420, 126569.

Feng, X., Jiao, Q., Chen, W., Dang, Y., Dai, Z., Suib, S.L., Zhang, J., Zhao, Y., Li, H. and Feng, C. (2021) Cactus-like $NiCo_2S_4$@NiFe LDH hollow spheres as an effective oxygen bifunctional electrocatalyst in alkaline solution. Appl. Catal. B: Environ. 286, 119869.

Gholami, P., Khataee, A., Soltani, R.D.C., Dinpazhoh, L. and Bhatnagar, A. (2020) Photocatalytic degradation of gemifloxacin antibiotic using Zn-Co-LDH@biochar nanocomposite. J. Hazard. Mater. 382, 121070.

Guo, X.X., Hu, T.T., Meng, B., Sun, Y. and Han, Y.-F. (2020) Catalytic degradation of

anthraquinones-containing H_2O_2 production effluent over layered Co-Cu hydroxides: Defects facilitating hydroxyl radicals generation. Appl. Catal. B: Environ. 260, 118157.

He, J., Lai, C., Qin, L., Li, B., Liu, S., Jiao, L., Fu, Y., Huang, D., Li, L., Zhang, M., Liu, X., Yi, H., Chen, L. and Li, Z. (2020) Strategy to improve gold nanoparticles loading efficiency on defect-free high silica ZSM-5 zeolite for the reduction of nitrophenols. Chemosphere 256, 127083.

Hong, P., Wu, Z., Yang, D., Zhang, K., He, J., Li, Y., Xie, C., Yang, W., Yang, Y., Kong, L. and Liu, J. (2021) Efficient generation of singlet oxygen ($^1O_2$) by hollow amorphous Co/C composites for selective degradation of oxytetracycline via Fenton-like process. Chem. Eng. J. 421, 129994.

Jawad, A., Liao, Z., Zhou, Z., Khan, A., Wang, T., Ifthikar, J., Shahzad, A., Chen, Z. and Chen, Z. (2017) Fe-MoS_4: An effective and stable LDH-based adsorbent for selective removal of heavy metals. ACS Appl. Mater. Inter. 9(34), 28451-28463.

Jiang, Y., Xu, W., Liang, J., Shen, J., Fu, X., He, H., Yan, S. and Ren, X. (2021) Enhanced catalytic phenol hydroxylation by CuZnFeAl layered double hydroxides: synergistic effects of Cu^+ and oxygen vacancies. New J. Chem. 45(1), 179-188.

Khataee, A., Sadeghi Rad, T., Nikzat, S., Hassani, A., Aslan, M.H., Kobya, M. and Demirbaş, E. (2019) Fabrication of NiFe layered double hydroxide/reduced graphene oxide (NiFe-LDH/rGO) nanocomposite with enhanced sonophotocatalytic activity for the degradation of moxifloxacin. Chem. Eng. J. 375, 122102.

Lai, C., Huang, F., Zeng, G., Huang, D., Qin, L., Cheng, M., Zhang, C., Li, B., Yi, H., Liu, S., Li, L. and Chen, L. (2019) Fabrication of novel magnetic $MnFe_2O_4$/bio-char composite and heterogeneous photo-Fenton degradation of tetracycline in near neutral pH. Chemosphere 224, 910-921.

Lai, C., Liu, S., Zhang, C., Zeng, G., Huang, D., Qin, L., Liu, X., Yi, H., Wang, R., Huang, F., Li, B. and Hu, T. (2018) Electrochemical aptasensor based on sulfur–nitrogen codoped ordered mesoporous carbon and thymine-Hg^{2+}-thymine mismatch structure for Hg^{2+} detection. ACS Sensors 3(12), 2566-2573.

Leng, M., Huang, X., Xiao, W., Ding, J., Liu, B., Du, Y. and Xue, J. (2017) Enhanced oxygen evolution reaction by Co-O-C bonds in rationally designed Co_3O_4/graphene nanocomposites. Nano Energy 35, 445-452.

Li, B., Lai, C., Lin, H., Liu, S., Qin, L., Zhang, M., Zhou, M., Li, L., Yi, H. and Chen, L. (2022a) The promising NIR light-driven MO_{3-x} (M = Mo, W) photocatalysts for energy conversion and environmental remediation. Chem. Eng. J. 431, 134044.

Li, B., Yu, S., Zhou, M., Chen, C., Lai, C., Zhang, M. and Lin, H. (2022b) Graphynes: the ideal supports of single atoms for electrochemical energy conversion. Journal of Materials Chemistry A. https://doi.org/10.1039/D1TA09659A.

Li, L., Lai, C., Huang, F., Cheng, M., Zeng, G., Huang, D., Li, B., Liu, S., Zhang, M., Qin, L., Li, M., He, J., Zhang, Y. and Chen, L. (2019) Degradation of naphthalene with magnetic bio-char activate hydrogen peroxide: Synergism of bio-char and Fe-Mn binary oxides. Water Res. 160, 238-248.

Li, L., Liu, S., Cheng, M., Lai, C., Zeng, G., Qin, L., Liu, X., Li, B., Zhang, W., Yi, Y.,

641 Zhang, M., Fu, Y., Li, M. and Long, M. (2021a) Improving the Fenton-like
642 catalytic performance of MnO_x-Fe_3O_4/biochar using reducing agents: A
643 comparative study. J. Hazard. Mater. 406, 124333.
644 Li, M., Li, P., Zhang, L., Chen, M., Tang, J., Qin, C., Ling Jie Lee, S. and Lin, S. (2022c)
645 Facile fabrication of ZnO decorated ZnFe-layered double hydroxides @ biochar
646 nanocomposites for synergistic photodegradation of tetracycline under visible
647 light. Chem. Eng. J. 434, 134772.
648 Li, S., Wang, H., Li, W., Wu, X., Tang, W. and Chen, Y. (2015) Effects of Cu substitution
649 on promoted benzene oxidation over porous CuCo-based catalysts derived from
650 layered double hydroxide with resistance of water vapor. Appl. Catal. B: Environ.
651 166-167, 260-269.
652 Li, T., Ge, L., Peng, X., Wang, W. and Zhang, W. (2021b) Enhanced degradation of
653 sulfamethoxazole by a novel Fenton-like system with significantly reduced
654 consumption of H_2O_2 activated by g-C_3N_4/MgO composite. Water Res. 190,
655 116777.
656 Liu, G., Zhang, Y., Yu, H., Jin, R. and Zhou, J. (2020) Acceleration of goethite-
657 catalyzed Fenton-like oxidation of ofloxacin by biochar. J. Hazard. Mater. 397,
658 122783.
659 Liu, H., Jiao, Q., Zhao, Y., Li, H., Sun, C. and Li, X. (2010) Mixed oxides derived from
660 Cu-Co layered double hydroxide nanorods: Preparation, characterization and their
661 catalytic activities. J. Alloy. Compd. 496(1), 317-323.
662 Liu, Y., Shi, S. and Wang, Y. (2021) Removal of pollutants from gas streams using

663 Fenton (-like)-based oxidation systems: A review. J. Hazard. Mater. 416, 125927.
664 Lu, H., Sui, M., Yuan, B., Wang, J. and Lv, Y. (2019) Efficient degradation of
665 nitrobenzene by Cu-Co-Fe-LDH catalyzed peroxymonosulfate to produce
666 hydroxyl radicals. Chem. Eng. J. 357, 140-149.
667 Lu, P., Lin, K. and Gan, J. (2020) Enhanced ozonation of ciprofloxacin in the presence
668 of bromide: Kinetics, products, pathways, and toxicity. Water Res. 183, 116105.
669 Luo, K., Yang, Q., Pang, Y., Wang, D., Li, X., Lei, M. and Huang, Q. (2019) Unveiling
670 the mechanism of biochar-activated hydrogen peroxide on the degradation of
671 ciprofloxacin. Chem. Eng. J. 374, 520-530.
672 Ma, W., Ma, R., Wang, C., Liang, J., Liu, X., Zhou, K. and Sasaki, T. (2015) A
673 superlattice of alternately stacked Ni-Fe hydroxide nanosheets and graphene for
674 efficient splitting of water. ACS Nano 9(2), 1977-1984.
675 Nosaka, Y. and Nosaka, A.Y. (2017) Generation and detection of reactive oxygen
676 species in photocatalysis. Chem. Rev. 117(17), 11302-11336.
677 Pan, J., Gao, B., Cao, Y., Duan, P., Guo, K., Akram, M., Xu, X. and Yue, Q. (2021) In-
678 situ Cu-doped carbon-supported catalysts applied for high-salinity polycarbonate
679 plant wastewater treatment and a coupling application. Chem. Eng. J. 416, 129441.
680 Peng, Y., Sun, Y., Hanif, A., Shang, J., Shen, Z., Hou, D., Zhou, Y., Chen, Q., Ok, Y.S.
681 and Tsang, D.C.W. (2021) Design and fabrication of exfoliated Mg/Al layered
682 double hydroxides on biochar support. J. Clean. Prod. 289, 125142.
683 Sathishkumar, K., Li, Y. and Sanganyado, E. (2020) Electrochemical behavior of
684 biochar and its effects on microbial nitrate reduction: Role of extracellular

685 polymeric substances in extracellular electron transfer. Chem. Eng. J. 395, 125077.
686 Sun, Y., Cho, D.-W., Graham, N.J.D., Hou, D., Yip, A.C.K., Khan, E., Song, H., Li, Y.
687 and Tsang, D.C.W. (2019) Degradation of antibiotics by modified vacuum-UV
688 based processes: Mechanistic consequences of H_2O_2 and $K_2S_2O_8$ in the presence
689 of halide ions. Sci. Total Environ. 664, 312-321.
690 Sun, Y., Yu, I.K.M., Tsang, D.C.W., Fan, J., Clark, J.H., Luo, G., Zhang, S., Khan, E.
691 and Graham, N.J.D. (2020) Tailored design of graphitic biochar for high-efficiency
692 and chemical-free microwave-assisted removal of refractory organic contaminants.
693 Chem. Eng. J. 398, 125505.
694 Tian, M., Liu, C., Neale, Z.G., Zheng, J., Long, D. and Cao, G. (2019) Chemically
695 bonding NiFe-LDH nanosheets on rGO for superior lithium-ion capacitors. Acs
696 Appl. Mater. Inter. 11(39), 35977-35987.
697 Wang, C., Gao, J. and Gu, C. (2017) Rapid destruction of tetrabromobisphenol A by
698 iron(III)-tetraamidomacrocyclic ligand/layered double hydroxide composite/H_2O_2
699 system. Environ. Sci. Technol. 51(1), 488-496.
700 Wang, D., Sun, Y., Tsang, D.C.W., Khan, E., Cho, D.-W., Zhou, Y., Qi, F., Gong, J. and
701 Wang, L. (2020a) Synergistic utilization of inherent halides and alcohols in
702 hydraulic fracturing wastewater for radical-based treatment: A case study of di-(2-
703 ethylhexyl) phthalate removal. J. Hazard. Mater. 384, 121321.
704 Wang, J., Liu, C., Feng, J., Cheng, D., Zhang, C., Yao, Y., Gu, Z., Hu, W., Wan, J. and
705 Yu, C. (2020b) MOFs derived Co/Cu bimetallic nanoparticles embedded in
706 graphitized carbon nanocubes as efficient Fenton catalysts. J. Hazard. Mater. 394,

122567.

Wang, Z., Lai, C., Qin, L., Fu, Y., He, J., Huang, D., Li, B., Zhang, M., Liu, S., Li, L., Zhang, W., Yi, H., Liu, X. and Zhou, X. (2020c) ZIF-8-modified $MnFe_2O_4$ with high crystallinity and superior photo-Fenton catalytic activity by Zn-O-Fe structure for TC degradation. Chem. Eng. J. 392, 124851.

Xin, S., Liu, G., Ma, X., Gong, J., Ma, B., Yan, Q., Chen, Q., Ma, D., Zhang, G., Gao, M. and Xin, Y. (2021) High efficiency heterogeneous Fenton-like catalyst biochar modified $CuFeO_2$ for the degradation of tetracycline: Economical synthesis, catalytic performance and mechanism. Appl. Catal. B: Environ. 280, 119386.

Yan, H., Lai, C., Wang, D., Liu, S., Li, X., Zhou, X., Yi, H., Li, B., Zhang, M., Li, L., Liu, X., Qin, L. and Fu, Y. (2021) In situ chemical oxidation: peroxide or persulfate coupled with membrane technology for wastewater treatment. J. Mater. Chem. A 9(20), 11944-11960.

Yang, F., Zhang, S., Sun, Y., Tsang, D.C.W., Cheng, K. and Ok, Y.S. (2019a) Assembling biochar with various layered double hydroxides for enhancement of phosphorus recovery. J. Hazard. Mater. 365, 665-673.

Yang, R., Zhou, Y., Xing, Y., Li, D., Jiang, D., Chen, M., Shi, W. and Yuan, S. (2019b) Synergistic coupling of CoFe-LDH arrays with NiFe-LDH nanosheet for highly efficient overall water splitting in alkaline media. Appl. Catal. B: Environ. 253, 131-139.

Ye, Q., Wu, J., Wu, P., Rehman, S., Ahmed, Z. and Zhu, N. (2021) Enhancing peroxymonosulfate activation by Co-Fe layered double hydroxide catalysts via

729 compositing with biochar. Chem. Eng. J. 417, 129111.
730 Ye, Q., Wu, J., Wu, P., Wang, J., Niu, W., Yang, S., Chen, M., Rehman, S. and Zhu, N.
731 (2020) Enhancing peroxymonosulfate activation of Fe-Al layered double
732 hydroxide by dissolved organic matter: Performance and mechanism. Water Res.
733 185, 116246.
734 Yi, H., Liu, S.Y., Lai, C., Zeng, G.M., Li, M.F., Liu, X.G., Li, B.S., Huo, X.Q., Qin, L.,
735 Li, L., Zhang, M.M., Fu, Y.K., An, Z.W. and Chen, L. (2021) Recent advance of
736 transition-metal-based layered double hydroxide nanosheets: Synthesis, properties,
737 modification, and electrocatalytic applications. Adv. Energy Mater. 11(14),
738 2002863.
739 Yuan, H.-Y., Ding, L.-J., Zama, E.F., Liu, P.-P., Hozzein, W.N. and Zhu, Y.-G. (2018)
740 Biochar modulates methanogenesis through electron syntrophy of microorganisms
741 with ethanol as a substrate. Environ. Sci. Technol. 52(21), 12198-12207.
742 Zhang, M., Lai, C., Li, B., Xu, F., Huang, D., Liu, S., Qin, L., Fu, Y., Liu, X., Yi, H.,
743 Zhang, Y., Ren, J. and Chen, L. (2020) Unravelling the role of dual quantum dots
744 cocatalyst in 0D/2D heterojunction photocatalyst for promoting photocatalytic
745 organic pollutant degradation. Chem. Eng. J. 396, 125343.
746 Zhao, M.-Q., Zhang, Q., Huang, J.-Q. and Wei, F. (2012) Hierarchical nanocomposites
747 derived from nanocarbons and layered double hydroxides-Properties, synthesis,
748 and applications. Adv. Funct. Mater. 22(4), 675-694.
749 Zhao, S. and Zhao, X. (2019) Insights into the role of singlet oxygen in the
750 photocatalytic hydrogen peroxide production over polyoxometalates-derived

metal oxides incorporated into graphitic carbon nitride framework. Appl. Catal. B: Environ. 250, 408-418.

Zhou, X., Zeng, Z., Zeng, G., Lai, C., Xiao, R., Liu, S., Huang, D., Qin, L., Liu, X., Li, B., Yi, H., Fu, Y., Li, L. and Wang, Z. (2020) Persulfate activation by swine bone char-derived hierarchical porous carbon: Multiple mechanism system for organic pollutant degradation in aqueous media. Chem. Eng. J. 383, 123091.

Zhuang, Y., Wang, X., Zhang, L., Dionysiou, D.D. and Shi, B. (2019) Fe-Chelated polymer templated graphene aerogel with enhanced Fenton-like efficiency for water treatment. Environ. Sci. Nano 6(11), 3232-3241.

761 Table 1 Surface area and pore characteristic of BC, Cu-Co LDH, and Cu-Co LDH/BC

Samples	Surface area (m^2/g)	Average pore size (nm)	Pore volume (cm^3/g)
BC	3.579	4.286	0.015
Cu-Co LDH	70.075	4.272	0.357
Cu-Co LDH/BC	87.537	3.439	0.269

762

763

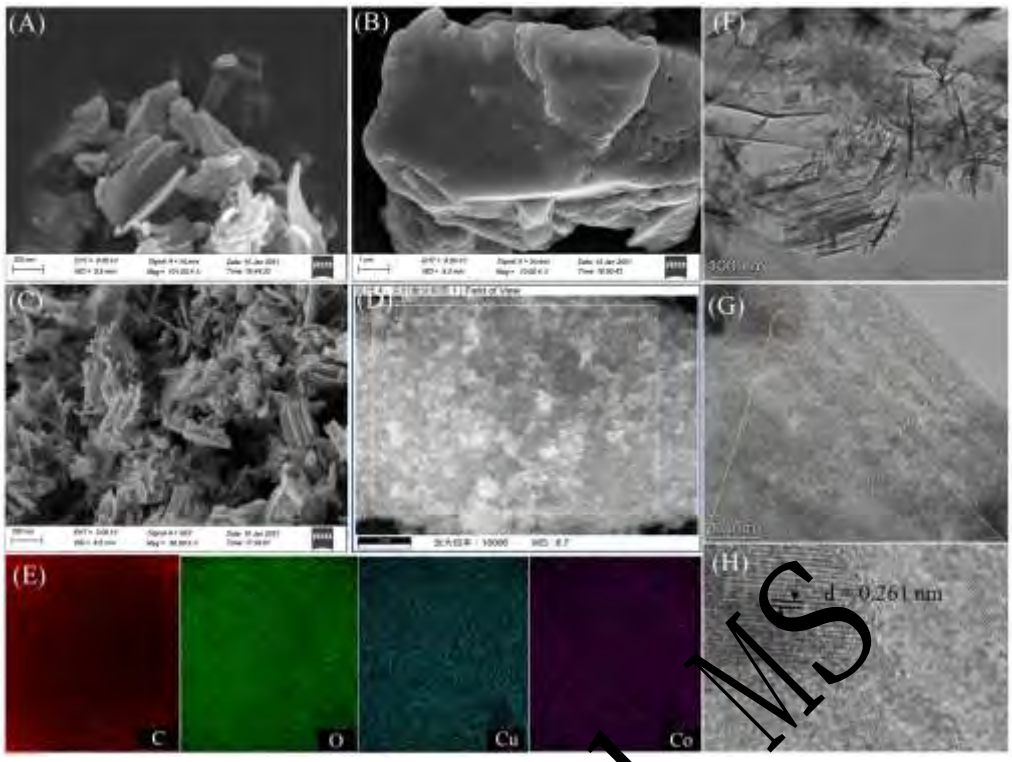

764

765 Fig. 1 SEM images of (A) Cu-Co LDH, (B) BC, (C-D) Cu-Co LDH/BC, (E) EDS-

766 elemental manning of Cu-Co LDH/BC, and TEM image of (F) Cu-Co LDH/BC, high-

767 resolution TEM image of Cu-Co LDH/BC (G-H).

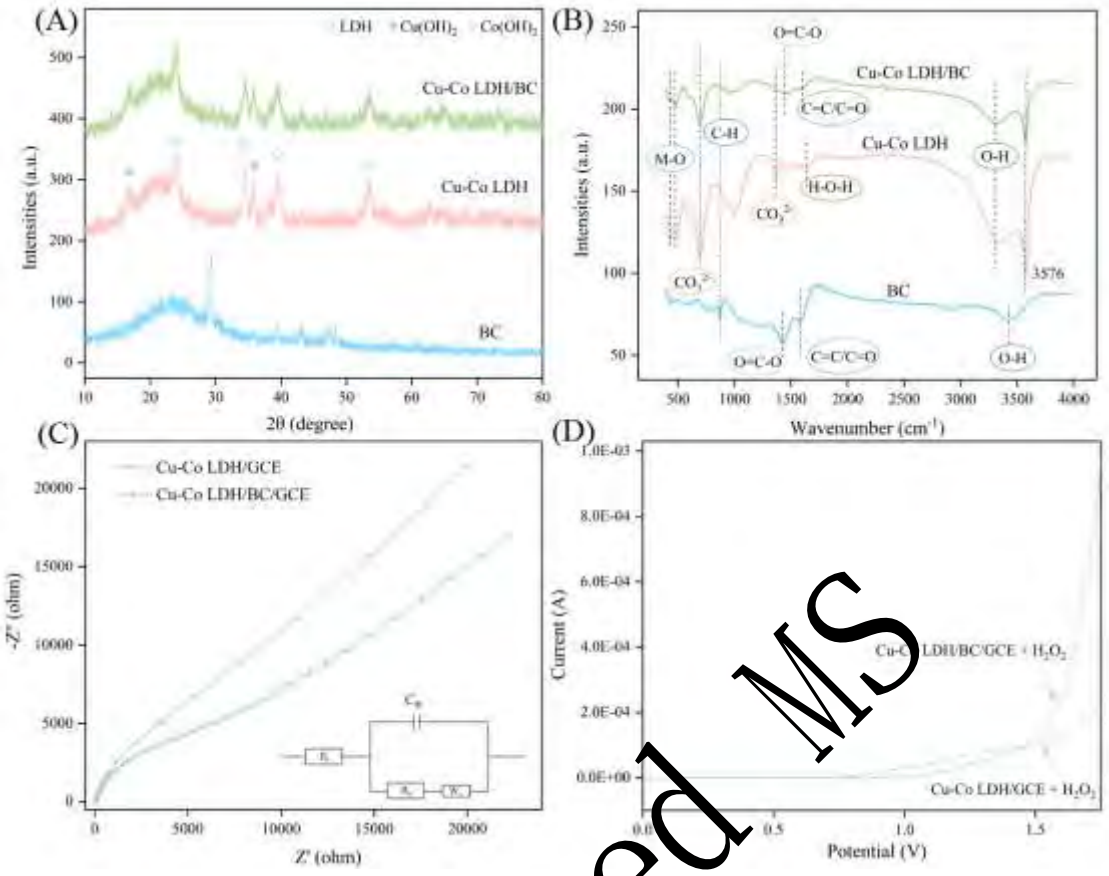

768

769 Fig. 2 (A) XRD patterns of BC, Cu-Co LDH, and Cu-Co LDH/BC, (B) FTIR spectra

770 of BC, Cu-Co LDH, and Cu-Co LDH/BC, (C) EIS Nyquist plots of Cu-Co LDH/Glassy

771 carbon electrode (GCE) and Cu-Co LDH/BC/GCE with frequency range from 0.01 Hz

772 to 10^5 Hz, and (D) LSV curves of Cu-Co LDH/GCE and Cu-Co LDH/BC/GCE in the

773 presence of H_2O_2.

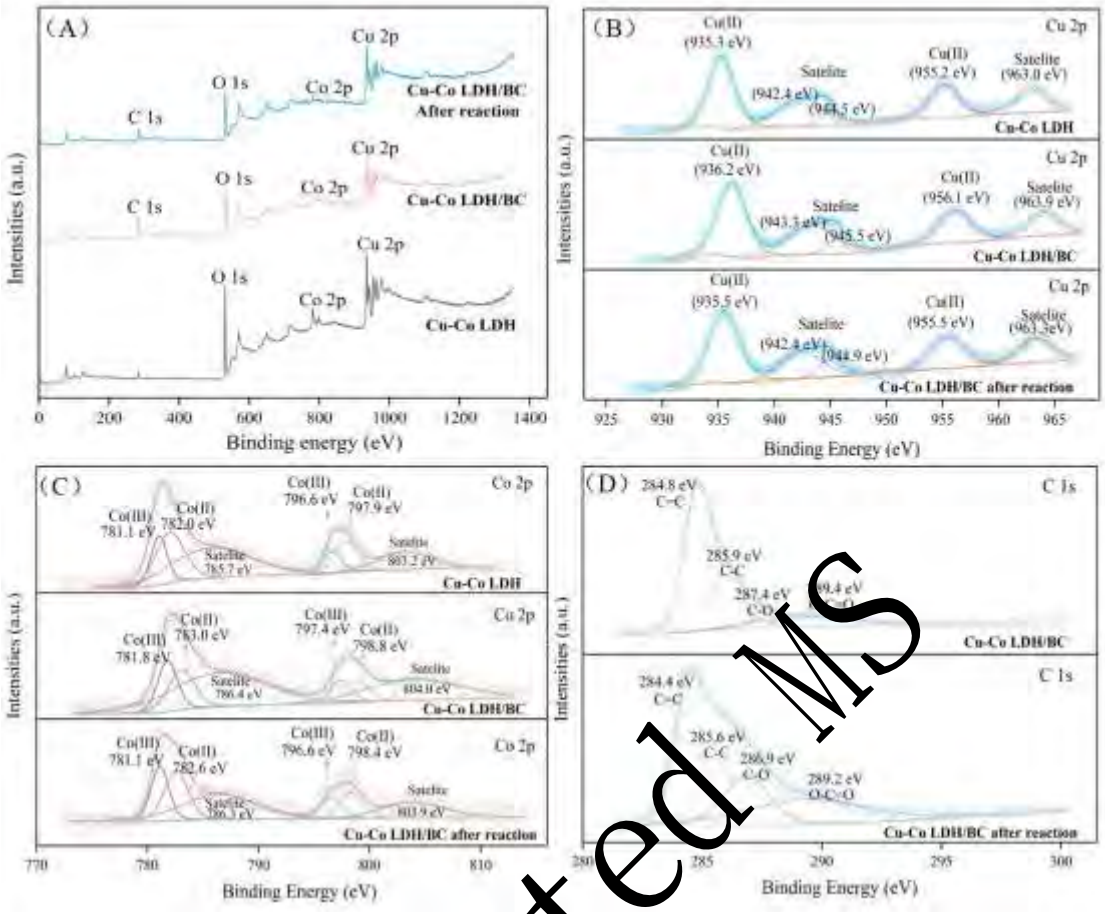

774

775 Fig. 3 (A) XPS survey, (B) Cu 2p spectra, (C) Co 2p spectra, and (D) C 1s spectra of

776 Cu-Co LDH, Cu-Co LDH/BC, and Cu-Co LDH/BC after reaction.

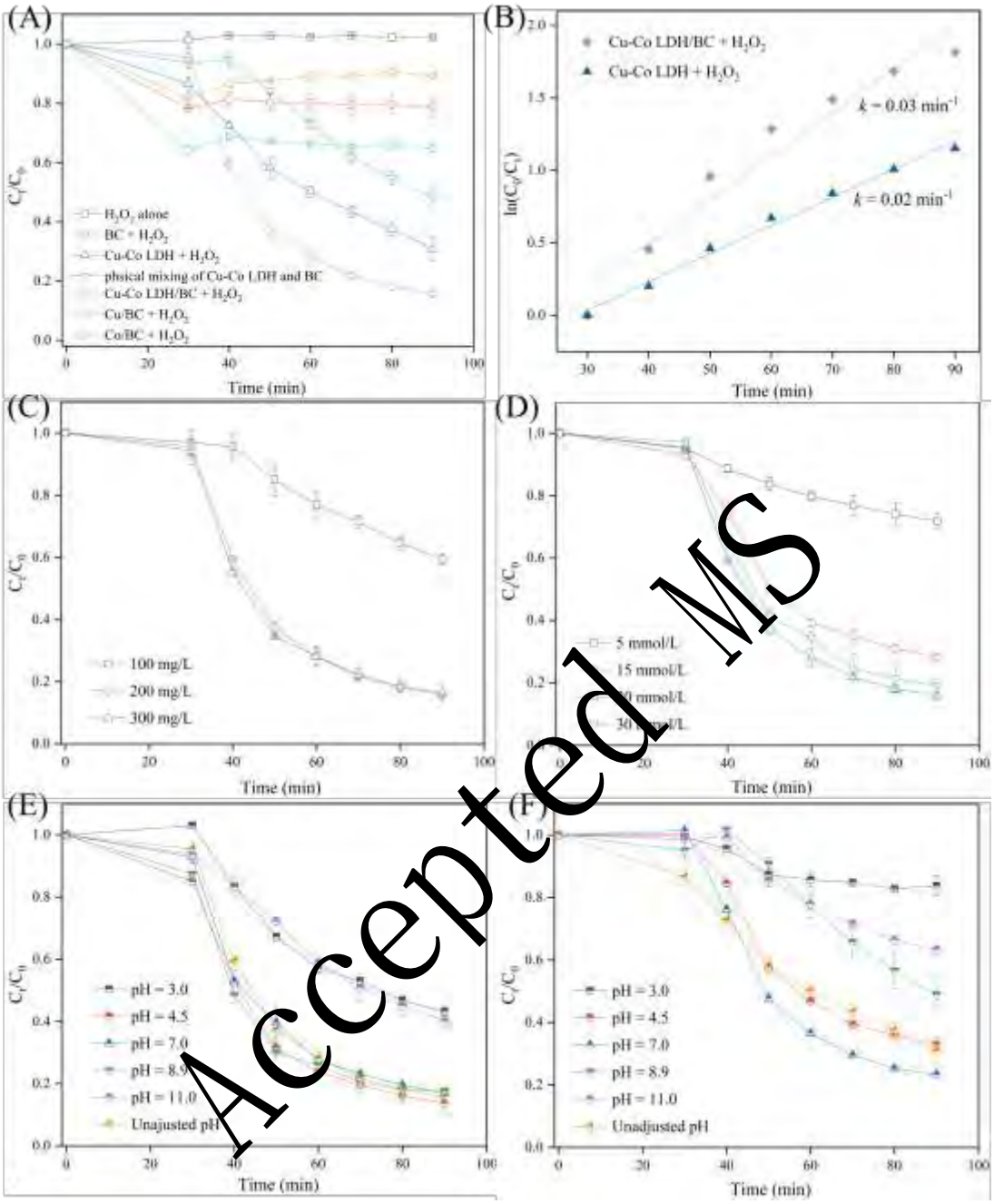

777

778 Fig. 4 (A) Degradation of CIP in different systems, (B) corresponding pseudo-first-
779 order kinetic fitting curves in different systems. Experimental conditions: catalyst
780 dosage = 200 mg/L (the dose of Cu-Co LDH and BC was 120 mg/L and 80 mg/L
781 respectively in the physical system); H_2O_2 concentration = 20 mmol/L; CIP
782 concentration = 10 mg/L; (C) Effects of catalyst dosage on Cu-Co LDH/BC.
783 Experimental conditions: H_2O_2 dosage = 20 mmol/L; CIP concentration = 10 mg/L; (D)

784 Effects of H_2O_2 dosage on Cu-Co LDH/BC. Experimental conditions: catalyst dosage
785 = 200 mg/L; CIP concentration = 10 mg/L; (E) Effects of solution pH on Cu-Co
786 LDH/BC, and (F) Effects of solution pH on Cu-Co LDH. Experimental conditions:
787 catalyst dosage = 200 mg/L; H_2O_2 concentration = 20 mmol/L; CIP concentration = 10
788 mg/L.

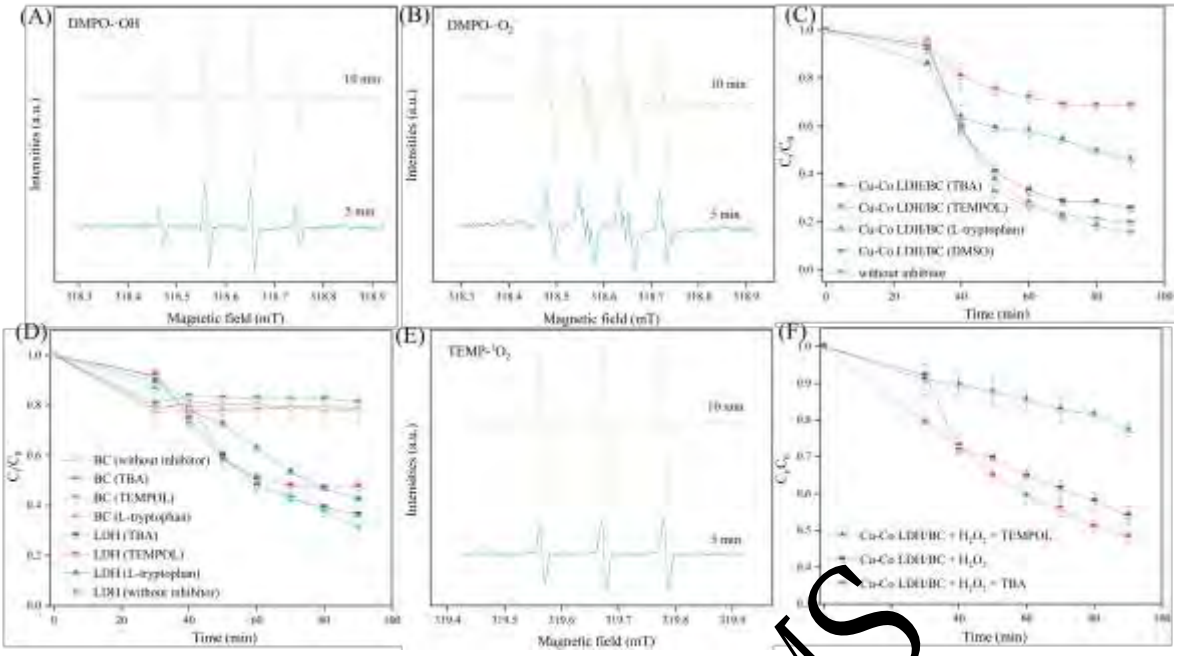

Fig. 5 The ESR spectra of (A) DMPO-·OH, (B) DMPO-$O_2^{\cdot-}$ in Cu-Co LDH/BC/H_2O_2 system; (C) The degradation curve of CIP with different inhibitors in Cu-Co LDH/BC/H_2O_2 system; (D) The degradation curve of CIP with different inhibitors in Cu-Co LDH/H_2O_2 and BC/H_2O_2 systems; Experimental conditions: catalyst dosage = 200 mg/L; H_2O_2 concentration = 20 mmol/L; CIP concentration = 10 mg/L; (E) The ESR spectra of TEMP-$^1O_2$ in Cu-Co LDH/BC/H_2O_2 system; and (F) The degradation curves of DPBF with Cu-Co LDH/BC in the presence of different scavengers. Experimental conditions: catalyst dosage = 200 mg/L; H_2O_2 concentration = 20 mmol/L; DPBF concentration = 0.05 mmol/L.

799

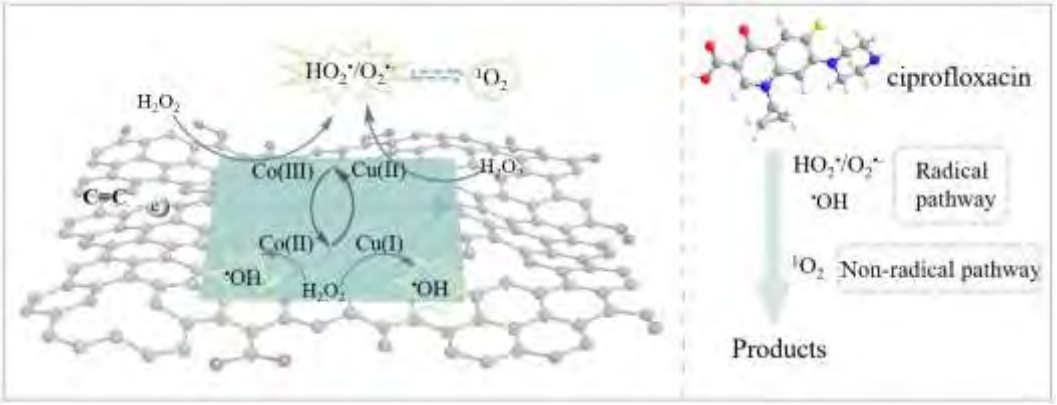

800 Fig. 6 The proposed reaction mechanism in Cu-Co LDH/BC/H_2O_2 system.

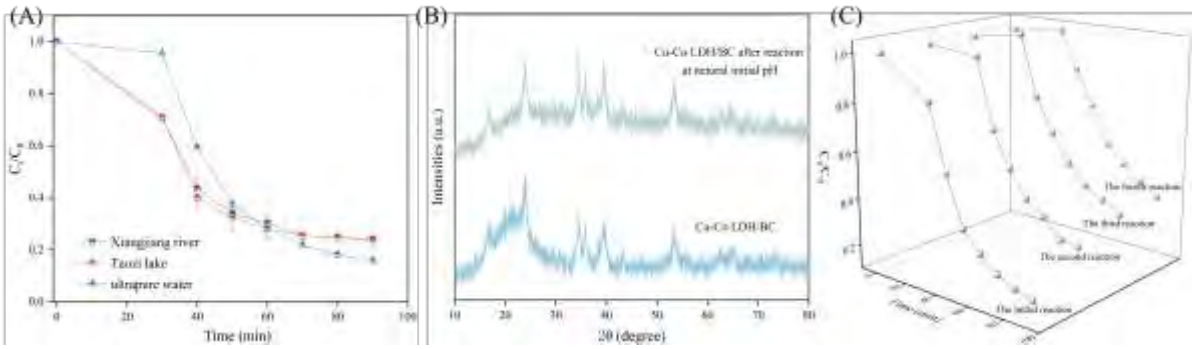

801

802 Fig. 7 (A) Degradation of CIP by Cu-Co LDH/BC in different water sources; (B) XRD

803 pattern of Cu-Co LDH/BC before and after reaction; and (C) The catalytic activity of

804 reused Cu-Co LDH/BC on CIP degradation. Experimental conditions: catalyst dosage

805 = 200 mg/L; H_2O_2 concentration = 20 mmol/L; CIP concentration = 10 mg/L.